Estimation for heterogeneous traffic using enhanced particle filters

Yanbing Wang[a] and Daniel B. Work[a]

[a]Department of Civil and Environmental Engineering and the Institute for Software Integrated Systems, Vanderbilt University, Nashville, TN 37240

ARTICLE HISTORY
Compiled November 12, 2021

ABSTRACT
This article explores the state estimation problem for heterogeneous traffic (a multi-class flow composed of vehicles with distinct sizes and driving behaviours) using particle filtering (PF) approaches. We consider three enhanced variations of the bootstrap PF to improve estimation. The benchmark PF utilises a deterministic partial differential equation and an additive process noise that is state-independent. For the enhanced variations we first consider a parameter-adaptive PF that also allows model parameters to be adjusted. The second variation is a standard PF with spatially-correlated noise. The last variation combines parameter-adaptive and the spatially-correlated-noise approaches. We compare the four filters in numerical experiments that represent complex heterogeneous traffic scenarios, as well as on real-world heterogeneous traffic data. The results show that the enhanced filters can achieve up to an 80% and 46% of accuracy improvement as compared to an open loop simulation without measurement correction, with the synthetic settings and with real traffic data, respectively. Moreover, the enhanced filters outperform the standard PF in all the traffic scenarios based on accuracy.

KEYWORDS
Traffic state estimation; Particle filter; Spatially-correlated noise modelling; Heterogeneous traffic

1. Introduction

Traffic is increasing in complexity around the world due to the diverse transportation modes and the distinct driving rules associated with each mode. Traffic control and management strategies depend on good estimation of traffic flow in spatial and temporal dimensions. While flow model based traffic management strategies are well developed for lane adhering homogeneous flows (Ferrara, Simona, and Silvia 2018), the modelling, estimation, and control of heterogeneous traffic is less well developed. The challenges for developing traffic control and management strategies to account for increasingly heterogeneous road users are many, and must be addressed to achieve accurate, safe and effective heterogeneous traffic management. These challenges include but are not limited to (1) much more complicated vehicular interactions that are difficult to capture from aggregate count or average speed data from traditional sensors; (2) lack of high quality heterogeneous traffic trajectory datasets to support

Yanbing Wang Email: yanbing.wang@vanderbilt.edu
Daniel B. Work Email: dan.work@vanderbilt.edu

research in this area. For example, although vehicle trajectory data for homogeneous traffic (NGSIM 2006; Krajewski et al. 2018) (see also (Li et al. 2020) for a recent review) are abundant, they do not contain heterogeneous traffic and vehicular interactions with loose lane-discipline; (3) there is no traffic estimation routine readily available for heterogeneous or loose lane-discipline traffic, due to the increasing nonlinearity of the traffic phenomena and the increased state space such that commonly used state estimators are prone to failure (Blandin et al. 2012). These limitations motivate a new generation of modelling and estimation techniques on complex traffic flows to be developed.

Various macroscopic traffic flow models have been proposed to extend seminal single class homogeneous models such as the *Lighthill-Whitham-Richards* (LWR) (Lighthill and Whitham 1955; Richards 1956) and *Aw, Rascle and Zhang* (ARZ) (Aw and Rascle 2000; Zhang 2002) models. One set of extensions describe multi-class traffic where vehicle classes follow homogeneous dynamics. Another set of extensions explicitly define vehicle dynamics which allow for bulk overtaking.

The growing interest for complex traffic has motivated studies on modelling traffic that is highly heterogeneous. These traffic flow models include, for example, the n-populations model (Benzoni-Gavage and Colombo 2002), which assumes that the average speed of a vehicle class depends on the mean free space and allows overtaking between vehicle classes. In a related work, the porous model (Nair, Mahmassani, and Miller-Hooks 2011) consider the heterogeneous traffic system as porous medium which allows small and fast vehicles to move through the 'pores' defined by the free space between other vehicles in a disordered flow. Another proposed model could capture overtaking in the free flow condition (Ngoduy and Liu 2007). The Fastlane model (van Lint, Hoogendoorn, and Schreuder 2008) introduces dynamic *passenger car equivalent* (PCE) parameters that scale according to the traffic state. The model of (Tang et al. 2009) considers the dynamics of traffic mixed with buses and cars. Algorithms are also developed to solve for multi-class traffic flow models, including (Zhang, Wong, and Shu 2006; Zhang et al. 2006; Zhang, Wong, and Xu 2008). Inspired by these works, the creeping model (Fan and Work 2015) explicitly defines class-specific velocity functions and jam densities to capture both overtaking and creeping features of heterogeneous traffic flows. More recently, a coupled microscopic-macroscopic model was proposed (Chalons, Monache, and Goatin 2017) to account for the effect of large and slow-moving vehicles, while the non-local multi-class traffic flow model (Chiarello and Goatin 2019) was developed to consider heterogeneous drivers and vehicles characterised by their look-ahead visibility. The porous model (Nair, Mahmassani, and Miller-Hooks 2011) was re-examined (Gashaw, Goatin, and Härri 2018) with an analytical expression for the pore space distribution such that the model is specifically tailored to a mixed flow of cars and powered two-wheelers.

The development of these new models are essential to incorporate the increasingly heterogeneous transportation environment present in different parts of the world. Other traffic modelling methods considering heterogeneous traffic, for example, include the multi-class model based on three dimensional flow concentration surface (Mohan and G.Ramadurai 2019), multi-class multi-lane mesoscopic modelling (Costeseque and Duret 2016), and cellular automata modelling (Mallikarjuna and Rao 2009). More detailed reviews of these and other models can be found in (van Wageningen-Kessels et al. 2015; Garavello, Han, and Piccoli 2016; Ferrara, Simona, and Silvia 2018).

For traffic control and management, accurate traffic state estimation is an important task. The problem is typically posed as a model-based estimation problem in which real-time data streams are used to correct model-based predictions in an online setting.

Kalman filter (KF) and the *extended Kalman filter* (EKF) was first proposed for traffic state estimation (Gazis and Knapp 1971; Szeto and Gazis 1972). The EKF is an extension of the KF for differentiable nonlinear systems and has since been broadly applied to traffic state estimation (Wang and Papageorgiou 2005; van Lint, Hoogendoorn, and Hegyi 2008; Hegyi et al. 2006). For non-differentiable models such as the *cell transmission model* (CTM) or its extensions, the *unscented Kalman filter* (UKF) and the *ensemble Kalman filter* (EnKF) are also applied (Hegyi et al. 2006; Ngoduy and Sumalee 2010; Work et al. 2008; Blandin et al. 2012; Risso et al. 2020). These Kalman-based filters, however, are minimal variance estimators which limit their application on traffic estimation problems that can generate multi-modal error distributions (Blandin et al. 2012), even though error bounds can be derived (Sun and Work 2017; Vivas et al. 2015; Sun and Work 2018). Therefore, a fully Monte Carlo sampling-based filter, the particle filter (Doucet and Johansen 2009; Chen 2003) is adopted (Mihaylova, Boel, and Hegyi 2007; Mihaylova et al. 2012; Wright and Horowitz 2016; Wang, Li, and Work 2017; Polson and Sokolov 2018). Readers can refer to a complete review on traffic estimation techniques and the associated flow models in (Seo et al. 2017).

We also notice that complementary approaches on existing filters can improve the state estimation performance. Demonstrated in (Mihaylova, Boel, and Hegyi 2007), a realistic Poisson distributed noise modeling is used to describe the empirical distribution of the field data. In (Boel and Mihaylova 2006), the randomness is introduced on the sending and receiving functions as well as on the speed adaptation rules to incorporate the stochasticity of the traffic model. Moreover, joint parameter-state estimation with a random walk parameter dynamic has shown to improve state estimation (Wang and Papageorgiou 2005); similar ideas related to dual filtering have also been explored for simultaneous parameter and state estimation (Hegyi et al. 2006; van Lint, Hoogendoorn, and Hegyi 2008).

Unlike the widely studied homogeneous traffic flow estimation problem, only a very small number of works consider multi-class traffic state estimation, e.g., (van Lint, Hoogendoorn, and Hegyi 2008; Ngoduy and Sumalee 2010; Ngoduy 2008). This is in part due to the increased complexity both in terms of the number of state variables (which increases proportionally with the number of classes), as well as the dynamics of the state variables (e.g., due to classes behaving distinctly in response to vehicles ahead). In (van Lint, Hoogendoorn, and Hegyi 2008), a dual EKF approach is considered to estimate the total density (and also the Fastlane model parameters), from which the individual class densities are recovered via their respective passenger car equivalents. In (Ngoduy 2008), an UKF is considered to track multi-class traffic in which overtaking is permitted in freeflow traffic but not congestion. In (Ngoduy and Sumalee 2010) an adaptive unscented Kalman filter that allows the model noise covariance matrix to be estimated simultaneous with the states is shown to outperform the standard UKF when applied to freeway traffic composed of cars and trucks.

Building on these works, in this article we consider the problem of traffic state estimation when the base traffic flow is heterogeneous and nontrivial interactions such as overtaking occur between classes. The traffic flow dynamics are described by the two-class creeping model (Fan and Work 2015), which allows small vehicles (e.g., motorbikes) to overtake larger ones, including when the large vehicles come to a complete stop. Traffic state estimation is performed using one of several fully nonlinear particle filtering algorithms. Because heterogeneous traffic may have significantly different operating rules compared to a homogeneous passenger-car traffic environment, we investigate the ability of each of the particle filters to reconstruct multi-class traffic in both simulated and real settings where overtaking of large vehicles by small vehicles can occur, particularly in highly congested traffic.

The main contribution of our work is to estimate class-specific heterogeneous traffic when nontrivial interactions occur. Compared to our preliminary work (Wang and Work 2019), in this article we propose and analyze three enhanced particle filtering techniques and consider their performance on complex multi-class traffic. In addition to the particle filter, we consider a parameter-adaptive filter that allows the model parameters to be adjusted at each step in parallel with the state estimation. We also consider a modification that enhances the standard particle filter with spatially correlated noise modelling as opposed to an independent process noise. Finally we combine the parameter adaptive filter with the spatially correlated process noise. We show that one can extract additional performance in the estimation using methods that are complementary to the more rigorous noise modeling approaches considered in (Mihaylova, Boel, and Hegyi 2007). We compare the enhanced filters with the standard bootstrap particle filter and provide detailed numerical studies on the performance of each of the four filters. The synthetic experimental results demonstrate that the enhanced filters, especially with spatially-correlated noise, can achieve up to 80% error reduction compared to a pure model-based forward simulation using the same dynamics assumed in the estimator. Compared to the standard particle filter, we demonstrate that the enhanced techniques can lead to performance improvements of up to 60%, depending on the traffic regime under which the complex traffic is estimated. The proposed enhanced filters are also assessed using a heterogeneous traffic data set (Kanagaraj et al. 2015). The results show that the enhanced filters can achieve up to 46% higher traffic reconstruction accuracy as compared to the forward simulation, which is in agreement with the synthetic testing scenarios.

The remainder of the article proceeds as follows. We briefly summarise the multi-class creeping traffic flow model used in the estimator, and the Bayesian state estimation framework in Section 2. Section 3 summarises the standard particle filter and introduces the enhanced methods. In the numerical experiments presented in Section 4, we evaluate the performance of the particle filter and its enhanced versions on four synthetic traffic scenarios. The proposed filters are further evaluated using real heterogeneous traffic data in Section 5 Finally, the conclusion and potential future works are highlighted in Section 6.

2. Preliminaries

In this section, we briefly review the two-class creeping model and the Bayesian state estimation framework for the construction of a model based estimator.

2.1. *A two-class creeping model*

The two-class creeping model (Fan and Work 2015) is a system of scalar conservation laws that governs the flow of each vehicle class:

$$\frac{\partial \rho_j(x,t)}{\partial t} + \frac{\partial \rho_j(x,t) V_j(r(x,t))}{\partial x} = 0, \; j \in \{1,2\}, \tag{1}$$

where $\rho_j(x,t)$ denotes the density of each vehicle class (indexed by j) at time t and space x. The velocity function for each class $V_j(\cdot)$ is distinct for each vehicle class and depends on the total density $r = \sum_j \rho_j$. For simplicity, in this work we consider the following velocity functions:

$$V_j(r) = \max\left(v^m\left(1 - \frac{r}{r_j^m}\right), 0\right),\ j \in \{1,2\} \tag{2}$$

where v^m is the speed limit applied to all road users. The class specific jam densities $r_j^m \in \{r_1^m, r_2^m\}$ control the total density r at which the individual vehicle classes come to a complete stop. If $r_1^m \neq r_2^m$, then one vehicle class will be able to creep through traffic while the other class is completely stopped. In the simplified setting considering a piecewise linear velocity function, the three parameters, v^m, r_1^m and r_2^m, completely define the two class creeping flow. Note that the creeping model is well posed (Fan and Work 2015), which is, in general, difficult to establish for many macroscopic models in which overtaking occurs.

Note that the model is able to capture a variety of traffic regimes such as overtaking (i.e., faster vehicles overtaking slower ones) and creeping (small vehicles overtaking large vehicles that have come to a complete stop). In multi-class traffic, the traffic regimes can be further complicated, for example, when one class is congested but the other class remains in free flow. Consequently, estimation on selected combinations of traffic regimes are tested in Section 4.

A numerical scheme is used to approximate the solution to the PDE (1) based on the Godunov scheme (Godunov 1959), which requires solving a Riemann problem at every interface between each pair of consecutive and discretised road segments at each time step. On scalar models, the approach leads to the well known *cell transmission model* (CTM) (Daganzo 1994, 1995). The discretised creeping model reads as follows:

$$\rho_{i,j}^{k+1} = \rho_{i,j}^{k} + \frac{\Delta t}{\Delta x}\left(F_{i-\frac{1}{2},j}^{k} - F_{i+\frac{1}{2},j}^{k}\right),\ j \in \{1,2\}, \tag{3}$$

where $\rho_{i,j}^k$ represents the density of class j in the ith cell at time k. The terms $F_{i-1/2,j}^k$ and $F_{i+1/2,j}^k$ are the numerical fluxes of class j via the upstream and downstream boundaries of cell i at time k.

For simplicity of the notation, we use subscripts on variables, e.g., $\rho_{-,j}$ and $\rho_{+,j}$, to represent upstream and downstream densities respectively of class j. The flux for vehicle class j over a cell boundary is thus defined as:

$$\begin{aligned} &F_j(\rho_{-,1}, \rho_{-,2}, \rho_{+,1}, \rho_{+,2}) \\ &\quad = \min\{S_j(\rho_{-,1}, \rho_{-,2}), R_j(\rho_{+,1}, \rho_{+,2})\},\ j \in \{1,2\}, \end{aligned} \tag{4}$$

where $S_j(\cdot,\cdot)$ and $R_j(\cdot,\cdot)$ are the sending and receiving functions for vehicle class j defined as:

$$S_j(\rho_{-,1}, \rho_{-,2}) = \begin{cases} Q_j(\rho_{-,1}, \rho_{-,2}) & \text{if } \rho_{-,j} \leq \rho_j^c(\rho_{-,\hat{j}}) \\ Q_j^{\max}(\rho_{-,\hat{j}}) & \text{if } \rho_{-,j} > \rho_j^c(\rho_{-,\hat{j}}) \end{cases} \tag{5}$$

$$R_j(\rho_{+,1}, \rho_{+,2}) = \begin{cases} Q_j^{\max}(\rho_{+,\hat{j}}) & \text{if } \rho_{+,j} > \rho_j^c(\rho_{+,\hat{j}}) \\ Q_j(\rho_{+,1}, \rho_{+,2}) & \text{if } \rho_{+,j} \leq \rho_j^c(\rho_{+,\hat{j}}), \end{cases} \tag{6}$$

where $\rho_{\hat{j}}$ denotes the density of the other vehicle class. In addition, $Q_j(\rho_1, \rho_2) =$

$\max\{\rho_j V_j(\rho_1+\rho_2), 0\}$, $Q_1^{\max}(\rho_2) = \max_{\rho_1} Q_1(\rho_1, \rho_2)$ and $\rho_1^c(\rho) = \frac{r_1^m - \rho_2}{2}$ is the critical density of ρ_1 such that $Q_1^{\max}$ is obtained. Similarly, $Q_2^{\max}(\rho_1) = \max_{\rho_2} Q_2(\rho_1, \rho_2)$ and $\rho_2^c(\rho) = \frac{r_2^m - \rho_1}{2}$ is the critical density of ρ_2 such that $Q_2^{\max}$ is obtained.

For a complete description and analysis of the model, the reader is referred to (Fan and Work 2015).

2.2. *Bayesian traffic state estimation*

The Bayesian approach to traffic state estimation evaluates the posterior distribution of the system state given a prior state estimate and measurement data. The state of the system $\boldsymbol{x}^k$ for model (3) at time k is defined as:

$$\boldsymbol{x}^k = \left[\rho_{1,1}^k, \ldots, \rho_{i_{\max},1}^k, \rho_{1,2}^k, \ldots, \rho_{i_{\max},2}^k\right]^T, \tag{7}$$

where $i_{\max}$ is the number of cells in the discretisation.

The state propagation equation is:

$$\boldsymbol{x}^k = f(\boldsymbol{x}^{k-1}, \boldsymbol{\theta}) + \boldsymbol{w}^k, \tag{8}$$

where $f(\cdot,\cdot)$ is the discrete-time creeping model defined in (3), and it propagates the traffic state to the next time step, with the input parameter vector $\boldsymbol{\theta} = [v^m, r_1^m, r_2^m]^T$. The measurement equation is:

$$\boldsymbol{y}^k = h(\boldsymbol{x}^k) + \boldsymbol{v}^k, \tag{9}$$

where $\boldsymbol{y}^k$ is the sensor data obtained at time k and relates to the system state through the measurement equation $h(\cdot)$. In the case when (a subset of) the system state is directly measured, the observation equation is linear. The terms $\boldsymbol{w}^k \sim \mathcal{N}(0, Q)$ and $\boldsymbol{v}^k \sim \mathcal{N}(0, R)$ denote the additive unbiased process noise and measurement noise at time k with assumed covariance matrices Q and R.

The state estimation problem can be viewed as sequentially evaluating the prior state distribution $p(\boldsymbol{x}^k|\boldsymbol{Y}^{k-1})$ and the posterior state distribution $p(\boldsymbol{x}^k|\boldsymbol{Y}^k)$ given measurements $\boldsymbol{Y}^k = [\boldsymbol{y}^1, \boldsymbol{y}^2, \ldots, \boldsymbol{y}^k]$, according to:

$$\begin{aligned} p(\boldsymbol{x}^k|\boldsymbol{Y}^{k-1}) &= \int p(\boldsymbol{x}^k|\boldsymbol{x}^{k-1}) p(\boldsymbol{x}^{k-1}|\boldsymbol{Y}^{k-1}) d\boldsymbol{x}^{k-1} \\ p(\boldsymbol{x}^k|\boldsymbol{Y}^k) &= \frac{p(\boldsymbol{y}^k|\boldsymbol{x}^k) p(\boldsymbol{x}^k|\boldsymbol{Y}^{k-1})}{p(\boldsymbol{y}^k|\boldsymbol{Y}^{k-1})}. \end{aligned} \tag{10}$$

In the particle filter described next in Section 3, the probability distributions (10) are evaluated based on sequential Monte Carlo sampling.

3. Particle filter

In this section, we summarise the standard bootstrap *particle filter* (PF) and discuss the weight degeneracy as measured by the *effective particle size*. Then we propose two enhancement methods, namely parameter-adaptive filtering and spatially-correlated process noise modelling, to improve the PF estimation.

Due to the nonlinearity and non-differentiability of the process model (1), discontinuities in the traffic state can occur, which can generate a multi-modal state distribution and limit the performance of minimal variance estimators such as EKF and UKF. The challenge motivates the use of PF, with the idea of propagating and updating Monte Carlo samples sequentially to represent the full state distribution without restrictive assumptions on the system dynamics and the noise distribution.

The particle filter starts with a collection of N_p samples (referred to as particles) from the initial state probability density function $p(\boldsymbol{x}^0)$, where $\boldsymbol{x}^0$ is a random variable representing the state vector at time $k = 0$. Each realisation of the state vector is denoted as $\boldsymbol{x}_l^0$, $l = 1, \cdots, N_p$. At each time instant, the particles are propagated to the next time step using the discrete time process model $f(\boldsymbol{x}, \boldsymbol{\theta})$, i.e., the traffic flow model (3), to approximate the prior state distribution $\boldsymbol{x}^{k|k-1}$ at time k.

The state distribution is updated after measurements are obtained. Specifically, a weight (q_l) is assigned to each particle based on the conditional relative likelihood evaluated from the likelihood function $p(\boldsymbol{y}^k|\boldsymbol{x}^k)$. The posterior state distribution $\boldsymbol{x}^{k|k}$ is approximated by resampling the particles according to the new weight distribution. This step ensures that the heavier-weighted particles are more likely to be drawn from the probability density function while the total number of particles is preserved.

The number of samples influences the PF performance due to the well-known sample degeneracy problem on high-dimensional systems (Martino, Elvira, and Louzada 2017; Surace, Kutschireiter, and Pfister 2019). In the section 4.2.4, we explore the effect of the number of samples on effective sample size and estimation accuracy. A standard PF algorithm used in this work is summarised in Algorithm 1. For a complete description of the algorithm, readers can find standard references such as (Doucet and Johansen 2009) and (Simon 2006).

Algorithm 1 PF algorithm

Initialise: Draw $\boldsymbol{x}_l^{0|0}$ from $\mathcal{N}(\boldsymbol{\mu}^0, Q^0)$ for $l = 1 : N_p$
for k = *1:T* **do**
  State propagation:
  $\boldsymbol{x}_l^{k|k-1} = f(\boldsymbol{x}_l^{k-1|k-1}, \boldsymbol{\theta}) + \boldsymbol{w}_l^k$ for all l
  State update:
  Assign weight: $q_l \coloneqq p[(\boldsymbol{y}^k = \boldsymbol{y}^{k*})|(\boldsymbol{x}^k = \boldsymbol{x}_l^{k|k-1})]$
  Normalise weight: $q_l \coloneqq \frac{q_l}{\sum_{l=1}^{N_p} q_l}$
  Resample:
  Draw $\boldsymbol{x}_l^{k|k}$ with probability q_l
end

$\boldsymbol{\mu}^0$: mean of the initial state distribution
Q^0: initial state covariance matrix
$\boldsymbol{x}_l^{k|k-1}$: sample l from prior state distribution at time k
$\boldsymbol{x}_l^{k|k}$: sample l from posterior state distribution at time k
$\boldsymbol{w}_l^k$: a realisation of the process noise $\boldsymbol{w}^k \sim \mathcal{N}(0, Q)$, where Q is the covariance matrix of $\boldsymbol{w}^k$
$\boldsymbol{y}^{k*}$: a measurement at time k

3.1. *Effective particle size*

An important measure of the validity of the filter is the *effective particle size*, which is not frequently discussed in the traffic estimation literature despite its diagnostic importance. As explained in (Surace, Kutschireiter, and Pfister 2019), the particle filter requires a sample size that increases exponentially with respect to the increase in state space dimension in order to achieve a valid estimation performance. But even with an extremely large sample size, a 'curse of dimensionality' still occurs. The curse of dimensionality in the PF is due to the degeneracy of importance weights (only a few samples carry significant weights and all others weights are almost zero) in high dimensional spaces. A measure of the degree of degeneracy is the *effective particle size* (N_{eff}) (Martino, Elvira, and Louzada 2017), defined by:

$$N_{\text{eff}} \approx \left[\sum_{l=1}^{N_p} (q_l)^2 \right]^{-1} . \tag{11}$$

A low N_{eff} is an indicator of sample degeneracy and is to be avoided.

Throughout the numerical experiments presented in Section 4, we use N_{eff} to compare the performance of the filters in addition to the estimation accuracy.

3.2. *Filter enhancement*

3.2.1. Parameter-adaptive particle filtering (PAPF)

Inspired by the dual filtering approach for simultaneous state and model parameter estimation (Hegyi et al. 2006; van Lint, Hoogendoorn, and Hegyi 2008; Olivier, Huang, and Craig 2012), in this filter, we allow the estimated model parameters to be adjusted at each time step instead of having fixed values, i.e., we model the parameters as time-invariant (the dynamics do not change over time) with some noise as approached in the standard dual-filtering problems mentioned above. This gives the estimator extra flexibility that can potentially produce more accurate state estimates. The goal is not for online parameter estimation due to the challenge in identifiability analysis of a nonlinear and non-differentiable model, but simply allowing parameter estimates to be updated in motion to facilitate state estimation. We name this approach *parameter-adaptive particle filter*, or PAPF in the remaining of this article.

The PAPF includes an additional particle filter running in parallel with the state estimator to adjust the estimated parameters. In the parameter propagation step, the parameter samples are obtained by performing a random walk from the best estimated parameter in the previous timestep, $\hat{\boldsymbol{\theta}}^{k-1|k-1}$. In the parameter update step, the prior state distribution ($\boldsymbol{x}^{k|k-1}$) is approximated by propagating the best state estimate at the previous timestep ($\hat{\boldsymbol{x}}^{k-1|k-1}$) through the traffic flow model (3) with the parameter samples. The remaining parameter update step follows a similar approach described in Algorithm 1: each parameter sample is re-weighted according to the relative likelihood function $p(\boldsymbol{y}^k|\boldsymbol{x}^k)$ after measurements are obtained, and resampled according to the new weight distribution. The estimator of the posterior parameter distribution, $\hat{\boldsymbol{\theta}}^{k|k}$, proceeds next for the state update. The state estimation exactly follows Algorithm 1 with the exception that the parameter in the state propagation equation is now the best posterior parameter estimator, $\hat{\boldsymbol{\theta}}^{k|k}$, instead of a deterministic parameter $\boldsymbol{\theta}$. The detailed PAPF algorithm is summarised in Algorithm 2.

Algorithm 2 PAPF algorithm

Initialise:
Draw $\boldsymbol{x}_l^{0|0}$ from $\mathcal{N}(\boldsymbol{\mu}^0, Q^0)$ for $l = 1 : N_p$
Set $\hat{\boldsymbol{x}}^{0|0} = \boldsymbol{\mu}^0$ and $\hat{\boldsymbol{\theta}}^{0|0} = \boldsymbol{\theta}^0$
for k = *1:T* **do**
  Parameter propagation:
  $\boldsymbol{\theta}_m^{k|k-1} = \hat{\boldsymbol{\theta}}^{k-1|k-1} + \boldsymbol{\eta}_m^k$ for $m = 1 : N_m$
  Parameter update:
  $\boldsymbol{x}_m^{k|k-1} = f(\hat{\boldsymbol{x}}^{k-1|k-1}, \boldsymbol{\theta}_m^{k|k-1}) + \boldsymbol{w}_m^k$ for all m
  Assign weight: $q_m \coloneqq p[(\boldsymbol{y}^k = \boldsymbol{y}^{k*})|(\boldsymbol{x}^k = \boldsymbol{x}_m^{k|k-1})]$
  Normalise weight: $q_m \coloneqq \frac{q_m}{\sum_{l=1}^{N_m} q_m}$
  Resample:
  Draw $\boldsymbol{\theta}_m^{k|k}$ with probability q_m
  Update $\hat{\boldsymbol{\theta}}^{k|k}$

  State propagation:
  $\boldsymbol{x}_l^{k|k-1} = f(\boldsymbol{x}_l^{k-1|k-1}, \hat{\boldsymbol{\theta}}^{k|k}) + \boldsymbol{w}_l^k$ for all l
  State update:
  Assign weight: $q_l \coloneqq p[(\boldsymbol{y}^k = \boldsymbol{y}^{k*})|(\boldsymbol{x}^k = \boldsymbol{x}_l^{k|k-1})]$
  Normalise weight: $q_l \coloneqq \frac{q_l}{\sum_{l=1}^{N_p} q_l}$
  Resample:
  Draw $\boldsymbol{x}_l^{k|k}$ with probability q_l
  Update $\hat{\boldsymbol{x}}^{k|k}$
end
$\boldsymbol{\mu}^0$: mean of the initial state distribution
Q^0: initial state covariance matrix
$\boldsymbol{\theta}^0$: initial parameter values
$\boldsymbol{\eta}_m^k$: a realisation of the parameter noise $\boldsymbol{\eta}^k \sim \mathcal{N}(0, Q_\theta)$, where Q_θ is the covariance matrix of $\boldsymbol{\eta}^k$
N_m: number of parameter samples at each time step
$\hat{\boldsymbol{x}}^{k|k}$: a point estimate of the state at time k
$\hat{\boldsymbol{\theta}}^{k|k}$: a point estimate of the parameter at time k

3.2.2. Spatially correlated noise modelling (SCNM)

This approach differs from Algorithm 1 in terms of the process noise at time k, $\boldsymbol{w}^k \sim \mathcal{N}(0, Q)$. In the PF, we apply the commonly implemented assumption that Q is a diagonal matrix, indicating that the elements of the state vector $\boldsymbol{x}^k$ are uncorrelated. It is suggested by (Boel and Mihaylova 2006) that if the traffic in one cell is extremely congested, then the vehicles interact very often with each other, and their location and speed will be highly correlated. Motivated by this observation, we modify the covariance matrix of the process noise $\boldsymbol{w}^k$ to $Q(i, i')$ with off-diagonal terms, which represents the similarity between all possible pairs of cells (indexed by i and i'). We use a covariance expression $Q(i, i') = \exp\left(-\frac{|i-i'|}{d}\right) \times \sigma^2_{\boldsymbol{w}^k}$, where $\sigma_{\boldsymbol{w}^k}$ is the standard deviation of noise $\boldsymbol{w}^k$. The characteristic length-scale d is a measure of how far away two cells (i, i') need to be for the cell values to be uncorrelated. The correlation between two cells is assumed to depend solely on the relative distance of the pair instead of the absolute location of the cells.

In practice, the traffic state can be highly correlated in space, i.e., cells in freeflow traffic are likely to occur next to each other, and similarly with the congested flow. We encode this heuristic via correlation in the process noise to account for a similar traffic pattern in neighbouring cells, and decrease the correlation with respect to the relative distance as one would expect. The introduction of a spatially correlated process noise increases the correlation on the prior state distribution, and is shown in Section 4 to improve the effective particle size.

4. Numerical experiments

In this section, we assess the capability of the standard PF and the enhanced PFs to track heterogeneous traffic flows in complex scenarios when interactions between two vehicle classes occur. The following four PFs are to be tested:

(1) A standard PF with spatially uncorrelated noise and deterministic parameters (denoted as PF in the remaining of the article)
(2) Parameter-adaptive particle filter with uncorrelated noise (PAPF)
(3) PF with spatially-correlated noise modelling and fixed parameters (PF+SCNM)
(4) Parameter-adaptive particle filter with spatially-correlated noise (PAPF+SCNM)

All the experiments are conducted in a controlled environment where the *true state* is known. In each experiment, we use the creeping model (3) (*true model*) to simulate the *ground truth*, which is to be estimated. Then, we run a forward model simulation with an *approximate model*, which also uses a creeping model (3), but with initial conditions, boundary conditions, and model parameters that differ from those in the true model. In the approximate model, these errors are intentionally introduced to capture the fact that in real deployments on real world experiments, the models often contain errors in parameter choices and initial and boundary conditions, see (Kaipio and Somersalo 2006). Finally we use the same approximate model within each PF variation to estimate the state using noisy measurements of the true state. The performance of each PF is measured by the error reduced from pure forward simulation using the approximate model. The comparison to the forward simulation allows us to verify the performance of the filters listed above, beyond purely having a good model in the estimator.

4.1. *Overview: filters and traffic scenarios setup*

To assess the performance of each filter, we create numerical experiments that represent real-world heterogeneous traffic scenarios. We consider a stretch of a roadway discretised into $i_{\max} = 40$ cells and the experiments are run for $k_{\max} = 126$ time steps. The roadway is shared between two vehicle classes with the density of small creeping vehicles denoted by class $j = 1$, and the large vehicles are denoted by class $j = 2$.

All four PFs use the same approximate model. The parameters of the true model and the approximate model used for pure forward simulation and for filtering are set according to the values in Table 1. Note that for cases where the parameters are al-

Table 1. Model parameters for all the experiments. In the case of PAPF, the parameters in the last column are the initial values in the approximate model.

Parameter	True model	Approximate model
v^m	1.8	1.9
r_1^m	1.8	1.7
r_2^m	1.0	0.9

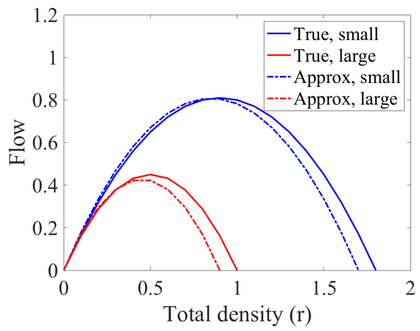

Figure 1. Fundamental diagrams of true and approximate models. The density and the flow values are normalised such that the jam density of the large vehicle class in the true model is 1.

lowed to be adjusted (PAPF and PAPF+SCNM), the approximate model parameter column records the initial values. The choice of true and approximate model parameters results in a slight difference in their corresponding fundamental diagrams, which can be visualised in Figure 1. In addition, the parameter-updating filter in Algorithm 2 uses a sample size $N_m = 1,500$ in parallel with the state update. For all four PFs, we consider that noisy density measurements for both vehicle classes are obtained in an upstream, intermediate, and downstream cells indexed by $i = 3, 20$, and 37, i.e., the measurement equation $h(\cdot)$ in (9) maps the state $\boldsymbol{x}^k$ to a 6×1 vector $\boldsymbol{y}^k$. The process noise and the initial noise are assumed to be Gaussian zero mean with a standard deviation of 0.05 and 0.06, respectively. We use the standard Gaussian white noise in the PF without any knowledge of the most suitable noise distribution a priori, but note that a more realistic noise distribution can be inferred from the data to improve the accuracy of state tracking (Mihaylova, Boel, and Hegyi 2007). The measurement noise follows a normal distribution with zero mean and 0.07 standard deviation. The boundary noises assumed in all PFs are bounded to prevent nonphysical (e.g., negative) density realisations on the boundary.

The four filters are evaluated on four selected characteristic tests which represent a subset of complex real-world traffic scenarios where interactions between vehicle classes occur. We consider *scenario 1*: overtaking traffic, *scenario 2*: congested traffic, *scenario 3*: queue clearance and *scenario 4*: creeping traffic. We first compare in detail of each filter's performance in the overtaking traffic condition, and then compare the filters on the rest of the traffic scenarios.

4.2. *Detailed comparison of the filters on overtaking traffic*

In this section we first briefly explain the initial and boundary conditions for the experimental setup, and then comment on the performance of the four filters with respect to the overall accuracy and the effective particle size. The traffic scenario considered in this case is when small vehicles (e.g., motorcycles or scooters) overtake large vehicles (e.g., cars and buses).

4.2.1. *Scenario 1: overtaking setup*

This set of experiment is designed to evaluate the filter performance when bulk overtaking occurs. The initial conditions are set such that the small fast vehicles begin behind the larger slower ones, and the downstream boundary conditions are set as free-flow so that both vehicle classes can freely exit the domain as the true state evolves. The upstream boundary conditions are assumed to oscillate at low densities.

The initial condition for the true model is given as:

$$\rho_{i,1}^{0} = \begin{cases} 0.5 & i \in [1,8] \\ 0 & \text{otherwise,} \end{cases} \quad \rho_{i,2}^{0} = \begin{cases} 0.6 & i \in [9,16] \\ 0 & \text{otherwise,} \end{cases} \tag{12}$$

which places the smaller faster vehicles initially behind the larger slower ones. The true upstream boundary conditions are assumed to oscillate at low densities:

$$\begin{aligned} \rho_{0,1}^{k} &= \operatorname{sgn}\left(\sin(0.07\ k)\right) \times 0.04 + 0.1 \\ \rho_{0,2}^{k} &= \operatorname{sgn}\left(\sin(0.07\ k)\right) \times 0.04 + 0.1. \end{aligned} \tag{13}$$

As the traffic evolves, the small vehicles beginning at the back of the queue overtakes the large vehicles and discharge downstream first. The true downstream conditions are set as empty, i.e., $\rho_{i_{\max}+1,1}^{k} = 0$, and $\rho_{i_{max}+1,2}^{k} = 0$.

In the approximate model used for forward simulation and for estimation, the initial conditions have errors compared to the true model (in addition to the parameter changes in Table 1). The initial condition in the approximate model is set as:

$$\hat{\rho}_{0,1}^{0} = \begin{cases} 0.7 & i \in [1,8] \\ 0 & \text{otherwise} \end{cases}, \quad \hat{\rho}_{0,2}^{0} = \begin{cases} 0.7 & i \in [9,16] \\ 0 & \text{otherwise,} \end{cases} \tag{14}$$

while the boundary condition is assumed to follow:

$$\begin{aligned} \hat{\rho}_{0,1}^{k} &= \operatorname{sgn}(\sin(0.07k)) \times 0.04 + 0.04 \\ \hat{\rho}_{0,2}^{k} &= \operatorname{sgn}(\sin(0.07k)) \times 0.04 + 0.04. \end{aligned} \tag{15}$$

Finally, in the approximate model we set a low-density downstream for both vehicle classes, i.e., $\hat{\rho}_{i_{max}+1,1}^{k} = 0.1$, and $\hat{\rho}_{i_{max}+1,2} = 0.1$.

4.2.2. *Filter performance: accuracy*

We now proceed to show the results of the filters. The *mean absolute error* (MAE) is used to quantify the overall error in density compared to the true state:

$$MAE_j = \frac{1}{k_{\max} \times i_{\max}} \sum_{i=1}^{i_{\max}} \sum_{k=1}^{k_{\max}} \mid \rho_{i,j}^{k} - \hat{\rho}_{i,j}^{k} \mid, \tag{16}$$

Table 2. Scenario 1: overtaking traffic. Filter results summary for $N_p = 1,500$.

		Average improvement (MAE reduce %)			
Scenario	Class	PF	PAPF	PF+SCNM	PAPF+SCNM
1	ρ_1	45.6	47.6	49.2	56.6
	ρ_2	2.89	23.5	44.8	48.8

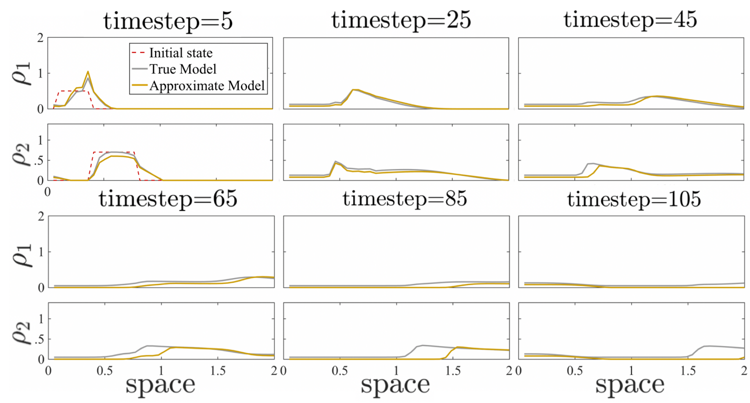

Figure 2. Scenario 1: overtaking traffic. Snapshots of the true state evolution and the forward simulation. The grey lines are the true states, and the gold lines are the predicted states by the approximate model.

where $\rho_{i,j}^k$ is the true state and $\hat{\rho}_{i,j}^k$ is the filter estimated state of vehicle class j at time k. We calculate the MAE of the forward simulation using the approximate model, and see how much MAE is reduced by running each filter.

Table 2 summarises the estimation result of each of the filters. We see that each of the enhanced PF produces a higher error reduction rate than the standard PF. The combination of the two enhancement methods, PAPF+SCNM, achieves a significant estimation accuracy (56.6% and 48.8% MAE reduction) compared to the standard PF (45.6% and 2.89% MAE reduction). This implies that the enhancement methods can greatly outperform the standard PF in the overtaking setting of the heterogeneous traffic.

From the forward simulation (Figure 2), we see that the performance of the filter is not due entirely to a 'good' model. In fact, the open loop simulation using the approximate model (Figure 2) differs and slowly drifts away from the true state evolution. By comparing to the forward simulation, all of the four filters are able to reduce the prediction error caused by the erroneous model in the estimator to various extents.

From Figures 3, we observe that the best filter (PAPF+SCNM shown in Figure 3(d)) tracks the true state evolution almost perfectly. In addition, the overtaking phenomenon between the two vehicle classes is correctly recovered by all four filters.

4.2.3. The effective particle size on the filter performance

Next we investigate the performance of each of the filters in terms of the effective particle size. Recall that in Section 3.1 we emphasise that the N_{eff} is an important measure of estimation validity. To demonstrate quantitatively the effective particle size obtained from each of the filters, Figure 4 shows the N_{eff} distribution for each of the filters. We see that the enhanced PFs, in general, are able to achieve a higher N_{eff} for the same number of total samples ($N_p = 1,500$) compared to the standard PF. Note that a higher N_{eff} allows the filter to capture the full state distribution without

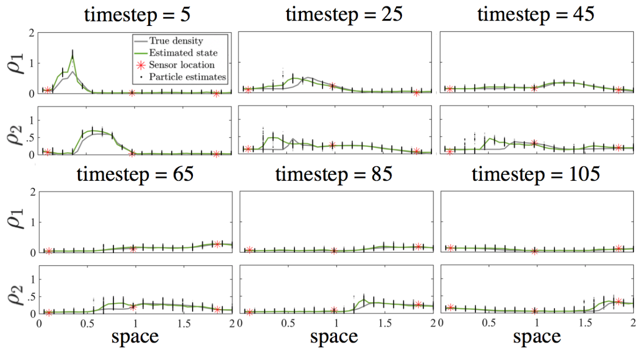

(a) PF

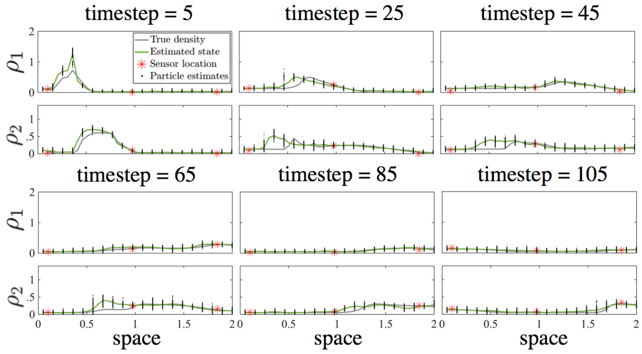

(b) PAPF

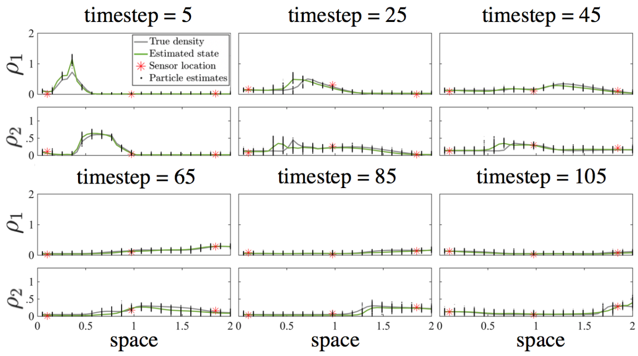

(c) PF+SCNM

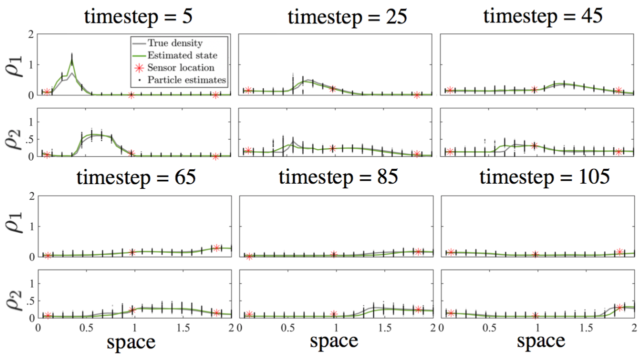

(d) PAPF+SCNM

Figure 3. Estimation results of scenario 1: overtaking traffic. Snapshots of (a) a standard PF and (b)-(d) enhanced PF estimates (green) compared to the true state evolution (grey).

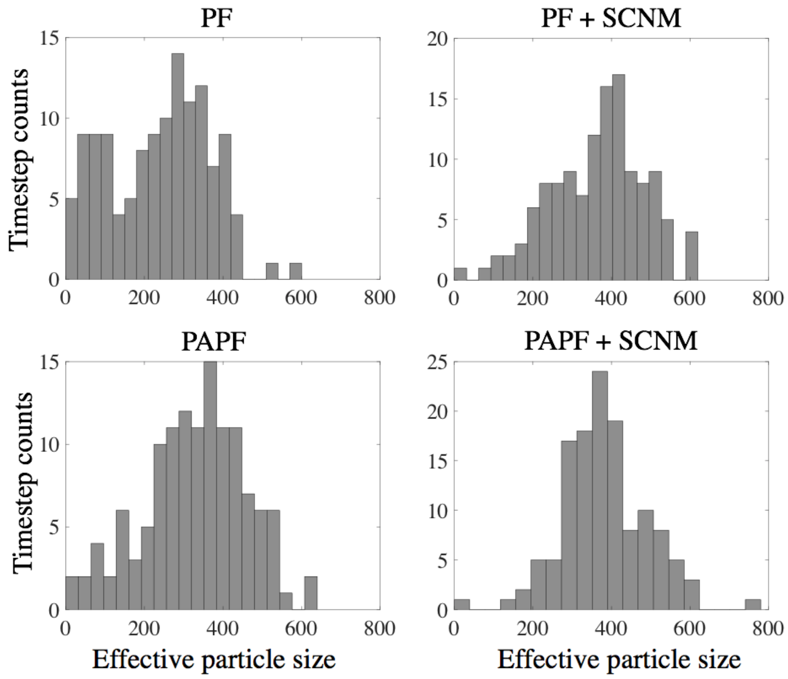

Figure 4. Scenario 1: overtaking traffic. Effective particle size histograms obtained from PF, PF+SCNM, PAPF and PAPF+SCNM using $N_p = 1,500$ particles.

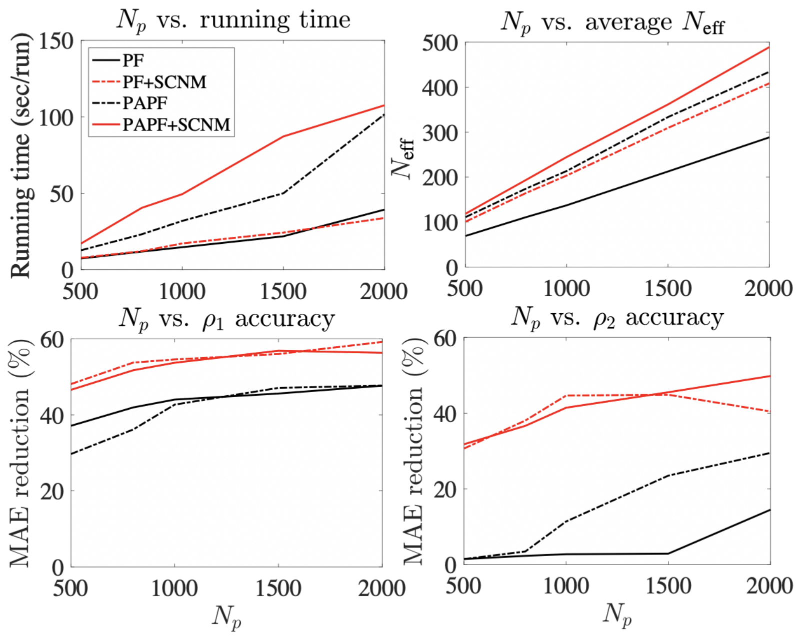

Figure 5. Scenario 1: overtaking traffic. Estimation results of 4 variations of PF with respect to the number of particles N_p.

collapsing. In the case of enhanced PFs (PF+SCNM, PAPF, and PAPF+SCNM), on average, approximately 400 out of 1500 particles carry the importance weights, whereas the standard PF only allows a handful of particles to carry the majority of the weight at some time-steps and thus is not a sufficient description of the state distribution.

4.2.4. The influence of sample size on the filter performance

Finally we conduct a series of experiments using different sample size (N_p), and analyze the total number of particles on the effective sample size, run time and accuracy of the four filters. Because the filter is stochastic, we conduct $N_r = 10$ filter runs for each selected N_p value between 500 to 2000. Figure 5 summarises the averaged results from the 10 runs.

From Figure 5, it is observed that the running time increases approximately linearly with respect to the sample size for all the PFs as expected, with the PF and PF+SCNM being almost equally fast. All the enhanced PFs (PAPF, PF+SCNM and PAPF+SCNM) achieve a higher N_{eff} compared to the standard PF. In addition, the enhanced PFs significantly improve the estimation accuracy compared to the standard PF for all the N_p values considered. Specifically, with only $N_p = 500$, both the PF+SCNM and PAPF+SCNM are able to achieve higher accuracy as that obtained from the standard PF using $N_p = 2,000$. In other words, both the PF+SCNM and PAPF+SCNM are able to achieve more than 100% MAE reduction compared to the standard PF. PF+SCNM stands out the most amongst all, with the fastest implementation and highest accuracy. This experiment illustrates the fact that the enhanced PFs ensure higher effective particle sizes and greatly improve estimation accuracy compared to the standard PF for all the N_p values considered.

All the numerical experiments performed in this work are produced using MATLAB® on a MacBook Pro with 2.7 GHz CPU. For each scenario, the running time per filter run ranges from 21 seconds for PF up to 92 seconds for SCNM+PAPF, with 1500 particles. We conducted 10 runs for each choice of sample size and each PF variation on four traffic scenarios. The source code for the numerical experiments is available at `https://github.com/Lab-Work/heterogeneous_traffic_estimation`.

4.3. *Filter performances in scenarios 2-4*

We test the PFs on additional scenarios to see if the results proceed to different traffic settings. The additional three scenarios follow the same roadway setup, number of particles, and the same choices of initial, process and measurement noises as the first scenario, the only differences being the initial and boundary conditions. We explore various settings of the initial and boundary conditions to capture the essence of the traffic evolution, such as the formation and dissipation of congestion (caused by e.g., change of computational domain and road geometry). Details of the experimental setup is summarised in Table 3 and 4.

We first describe the three remaining traffic scenarios, and then compare the performance of the enhanced PFs with the standard PF. Through numerical experiments, the enhanced PFs again show similar positive results in recovering heterogeneous traffic patterns under various vehicular interactions.

Table 3. Initial conditions

Scenario	True model	Approximate model
2	$\rho^0_{i,1} = \begin{cases} 0.1 & i \in [1,15] \\ 0.55 & i \in [16,22] \\ 0.1 & \text{otherwise} \end{cases}$ $\rho^0_{i,2} = 0.9$	$\hat{\rho}^0_{i,1} = \begin{cases} 0.2 & i \in [1,15] \\ 0.65 & i \in [16,22] \\ 0.2 & \text{otherwise} \end{cases}$ $\hat{\rho}^0_{i,2} = 0.7$
3	$\rho^0_{i,1} = \begin{cases} 1.4 & i \in [1,25] \\ 0 & \text{otherwise} \end{cases}$ $\rho^0_{i,2} = \begin{cases} 0.6 & i \in [1,25] \\ 0 & \text{otherwise} \end{cases}$	$\hat{\rho}^0_{i,1} = \begin{cases} 1.2 & i \in [1,25] \\ 0 & \text{otherwise} \end{cases}$ $\hat{\rho}^0_{i,2} = \begin{cases} 0.4 & i \in [1,25] \\ 0 & \text{otherwise} \end{cases}$
4	$\rho^0_{i,1} = \begin{cases} 0.4 & i \in [1,14] \\ 0 & \text{otherwise} \end{cases}$ $\rho^0_{i,2} = \begin{cases} 0.8 & i \in [15,40] \\ 0 & \text{otherwise} \end{cases}$	$\hat{\rho}^0_{i,1} = \begin{cases} 0.3 & i \in [15,40] \\ 0 & \text{otherwise} \end{cases}$ $\hat{\rho}^0_{i,2} = \begin{cases} 0.7 & i \in [15,40] \\ 0 & \text{otherwise} \end{cases}$

Table 4. Boundary conditions

Scenario	True model	Approximate model
2	$\rho^k_{0,1} = 0$ $\rho^0_{i,2} = 0.9.$ $\rho^k_{i_{max+1},1} = 0.1$ $\rho^k_{i_{max+1},2} = 0.9$	$\hat{\rho}^k_{0,1} = 0.1$ $\hat{\rho}^0_{i,2} = 0.7$ $\hat{\rho}^k_{i_{max+1},1} = 0.1$ $\hat{\rho}^k_{i_{max+1},2} = 0.7$
3	$\rho^k_{0,1} = 1.4$ $\rho^k_{0,2} = 0.6$ $\rho^k_{i_{max+1},1} = 0.2$ $\rho^k_{i_{max+1},2} = 0.2$	$\hat{\rho}^k_{0,1} = 1.2$ $\hat{\rho}^k_{0,2} = 0.4$ $\hat{\rho}^k_{i_{max+1},1} = 0.1$ $\hat{\rho}^k_{i_{max+1},2} = 0.1$
4	$\rho^k_{0,1} = \text{sgn}(\sin(0.07\ k)) \times 0.04 + 0.08$ $\rho^k_{0,2} = \text{sgn}(\sin(0.07\ k)) \times 0.04 + 0.08$	$\hat{\rho}^k_{0,1} = \text{sgn}(\sin(0.07\ k)) \times 0.04 + 0.04$ $\hat{\rho}^k_{0,2} = \text{sgn}(\sin(0.07\ k)) \times 0.04 + 0.04$

4.3.1. Overview of the additional traffic scenarios

(a) Scenario 2: congested traffic. This scenario describes a small portion of two-wheelers maneuver through the congested traffic. It assumes a highly congested regime and the two vehicle classes move at different speeds.
(b) Scenario 3: queue clearance. This experiment depicts a scene when traffic light turns green or a bottleneck is removed. Both vehicle classes start off being congested, and transition to free-flow so that congested traffic is allowed to freely dissipate downstream without interference.
(c) Scenario 4: creeping traffic. Similar to congested traffic, this experiment is designed to evaluate the filter performance in highly congested regime when the large and slow vehicles completely stop while the small and fast vehicles keep moving. The initial conditions are set such that the large vehicles begin ahead of the small creeping vehicles. The downstream boundary condition is sufficiently large to cause the large vehicles to come to a complete rest, while the smaller vehicles are still able to advance.

Table 5. Scenarios 2-4: filter results summary.

		Average improvement (MAE reduction %)			
Scenario	Class	PF	PAPF	PF+SCNM	PAPF+SCNM
2	ρ_1	27.9	32.2	54.4	51.4
	ρ_2	49.0	44.4	84.4	83.8
3	ρ_1	-90.3	-72.7	25.8	24.3
	ρ_2	0.37	19.4	68.7	65.2
4	ρ_1	4.23	7.72	26.8	27.7
	ρ_2	30.4	21.2	39.8	42.5

4.3.2. Discussion on the filter performance

The performance of each of the filters under three additional traffic scenarios is summarised in Table 5. From the results, we see that the enhanced PFs almost always outperform the PF. Notably in scenario 2, both the PF+SCNM and PAPF+SCNM reduce the MAE by 50-80% depending on the vehicle class, and accurately recover the true state. Moreover, the error is approximately half of the error achieved when running the standard PF. Another observation worth noting is that in Scenario 3: queue clearance where the traffic evolves from an initial condition that has congestion upstream and free flowing downstream, a PF with additive Gaussian uncorrelated noise is insufficient (shown -90% improvement compared to forward simulation with the approximate model). The positions where the estimates deviate most from the true states are upstream in the initially congested traffic. A significant improvement is observed when adding spatially correlated noise in Scenario 3, where the information captured at the sensor locations is shared in a wider neighbourhood cells due to the correlation, in line with the observation from (Boel and Mihaylova 2006).

We also observe that in most of the tested cases, PAPF outperforms the PF, but the improvement is not as pronounced as adding SCNM does, although it is shown in (Wang and Papageorgiou 2005) that state estimation improves particularly in the case of real-time changes of the traffic behavior when a ‘random walk’ dynamic is given to the unknown parameters. This is because the ability of a filter to estimate the parameters (parameter identifiability) is closely related to the state observability, which is a challenging issue even in the first-order macroscopic traffic dynamics (Blandin et al. 2012). Previous work (Sun and Work 2018) suggests that the estimation error bound in the presence of a shock for a simplified variation of the cell transition model can be derived, but the same strategies cannot be applied here due to fact that there is no straightforward way to recast the creeping model as a switched linear system. In particular, we observe that with parameter-adaptation, the convergence issue can be exacerbated in all cases. Without error bounds, the numerical experiments provide practical insight to the performance we can expect in different traffic contexts. An extensive study on heterogeneous model parameter identifiability might be needed to address the convergence issue.

From the numerical experiments considered in this work, we conclude that enhancements to the particle filter via spatially correlated noise modelling and parameter adaptation are promising directions to accurately reconstruct heterogeneous traffic.

5. Evaluation on real heterogeneous traffic data

In this section, we apply the enhanced particle filters on heterogeneous trajectory

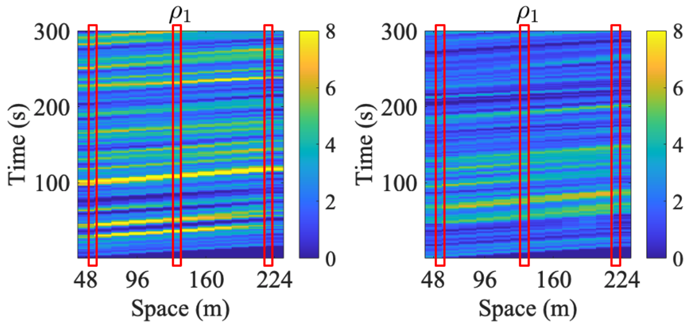

Figure 6. Density evolution of real heterogeneous traffic data. The red rectangles indicate measurement positions.

data collected in Chennai, India (Kanagaraj et al. 2015). We first briefly describe the dataset and preparation for the use of our proposed methods. Then, we describe the experiment setup including the estimated model parameters and particle filter parameters. Finally, we discuss the results.

5.1. *Data description and preparation*

In this study, we incorporate the vehicle trajectory data in mixed traffic (Kanagaraj et al. 2015). The dataset was extracted from the video sequences in an urban mid-block road section in Chennai, India. Various types of road users were present in the data, such as passenger vehicles, buses, motorbikes and auto-rickshaws. The data was prepossessed to include 3,005 vehicle trajectories, and the positions were recorded at a resolution of 0.5 s for 15 min on a stretch of 245 m, 3-lane city roadway. The total traffic flow observed in the study section is 6,010 vehicles per hour, and the instantaneous speeds vary from 0 to 15.22 m/s.

For the purpose of this study, we first discretise the densities such that $\Delta x = 16.3m$ (or $i_{max} = 15$) and $\Delta t = 1s$. We then count the number of occurrences of each vehicle in each discretised cell at each time step. We separate the counts of motorbikes (as the smaller, faster class, corresponding to ρ_1) and the counts of all other road agents combined (or the larger, slower class corresponding to ρ_2), because of motorbikes' observed overtaking properties. Lastly, a kernel density estimation (KDE) approach (Bowman and Azzalini 2000; Hill 1985) with a fixed Gaussian kernel is employed to transform the initial counts into macroscopic traffic quantities (e.g., density of each vehicle type, in number of vehicles per cell) across time and space. We use $\rho_{i,j}^k$ to denote the density of class j at cell i at time step k.

The obtained heterogeneous traffic density data can be visualised in Figure 6. It also serves as the 'ground truth' macroscopic traffic data for the state reconstruction tasks.

5.2. *Experiment setup*

Following a similar experiment setup in Section 4, the roadway is discretised into $i_{\max} = 15$ cells and the experiments are run for $k_{\max} = 300$ time steps, or 300 seconds. All four PFs use the same approxiamte model, with the specifications summarised in Table 7. Again for filters with parameter-adjustment (PAPF and PAPF+SCNM),

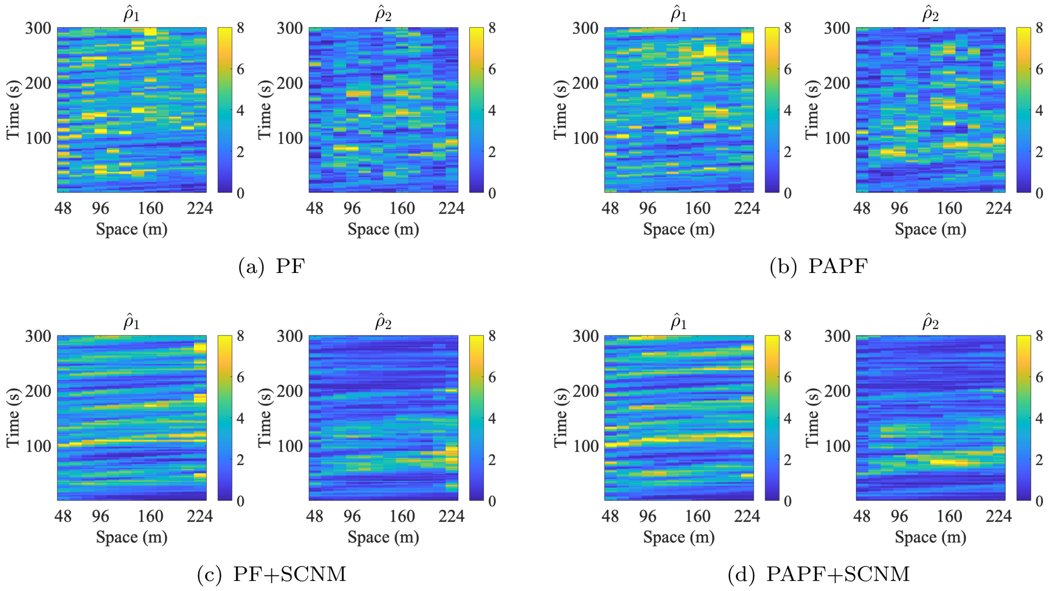

Figure 7. Filter performance: estimated density evolution

the approximate model parameters are the initial parameter estimates, and the noise on each parameter is assumed to follow a Gaussian zero mean and 0.005 standard deviation. In addition, both the parameter-update step and the state-update step use $N_p = 500$ particles, which is empirically shown as suitable for the state dimension. We assume that the noisy density measurements for both vehicle classes are obtained in an upstream, an intermediate and a downstream cells indexed by $i = 2, 8$ and 14, as indicated by the red rectangles in Figure 6. The initial state noise, the measurement noise and the state prediction noise are all assumed to be Gaussian zero mean, with standard deviation of 1 vehicle/cell. For filters with spatially correlated noise (PF+SCNM and PAPF+SCNM), a characteristic length of 15 is used.

Table 6. Initial and boundary conditions

Conditions	Approximate model
Initial conditions	$\hat{\rho}_{i,1}^0 = \begin{cases} 4 & i \in [1,8] \\ 1 & \text{otherwise} \end{cases}$
	$\hat{\rho}_{i,2}^0 = 1, \forall i$
Boundary conditions	$\hat{\rho}_{0,1}^k = \text{sgn}\left(\sin(0.4\ k)\right) \times 8 + 8$
	$\hat{\rho}_{0,2}^k = 1, \forall k$
	$\hat{\rho}_{i_{max}+1,1}^k = 2, \forall k$
	$\hat{\rho}_{i_{max}+1,1}^k = 2, \forall k$

In addition, we empirically choose the model initial and boundary conditions (Table 6) to best represent the observed measurements. The approximate model with the specified parameters, initial and boundary conditions is shown to yield MAEs of 1.92 and 1.67 vehicles/cell for class ρ_1 and ρ_2, respectively, in the studied space and time frame.

Table 7. Approximate model parameters

Parameter	Approximate model
v^m	15.3 m/s
r_1^m	16 vehicles/cell
r_2^m	10 vehicles/cell

Table 8. Filter performance summary on real data.

	Average improvement (MAE reduction %)			
Class	PF	PAPF	PF+SCNM	PAPF+SCNM
ρ_1	31.9	33.2	46.4	43.9
ρ_2	25.8	29.5	46.3	31.5

5.3. *Results and discussion*

The estimated density evolution from PF, PAPF, PF+SCNM and PAPF+SCNM can be visualised in Figure 7. A visual inspection indicates that filters with spatial correlation (PF+SCNM and PAPF+SCNM) generally have a more pronounced state reconstruction performance than PF and PAPF. The flow for both vehicle classes is 'smoother' across the space. Practically, spatial correlation in the states help to correct one part of the states, which carries over to its neighbourhoods. It models the similarity in densities of cells of close vicinity, which may implicitly capture the flow dynamics of traffic that PF without SCNM cannot capture.

It can also be observed that PAPF does not provide as significant improvement in traffic state reconstruction as SCNM does. This could be due to a combination of the identifiability issue of the creeping model parameters as well as observability issue of the state, which are not in the scope of this work. Since the recorded traffic is mostly in free-flow state, the filter performance cannot generalize to a variety of traffic regimes. When available, heterogeneous traffic data that contains traffic jams or creeping scenarios should be used to validate our proposed filters for various traffic state reconstruction.

Nevertheless, with the limited heterogeneous data available, the enhanced filters show significant improvement than the standard PF, and improve the estimation accuracy up to 46% as compared to using the approximate model alone. The findings using real heterogeneous data is also in agreement with the results from the numerical experiments: PF with parameter-adaptation and spatially-correlated noises are promising enhancement for traffic state estimation problems.

6. Conclusion

Considering previous traffic estimation works mainly focus on homogeneous flow with strict lane adherence, this work tackles estimation problem on heterogeneous traffic where non-trivial vehicular interactions occur. Due to the filtering challenges caused by the nonlinear and non-differentiable nature of the traffic flow model, in this article we propose three methods to enhance the standard particle filter to estimate complex traffic, both in simulated environments and with real heterogeneous traffic data. The results show that the enhanced PFs, especially with spatially-correlated noise modelling, can reduce the estimation error up to 80% and 46% from forward simulation using the approximate model, using the synthetic data and real data, respectively. The enhanced PFs significantly and consistently outperform the standard PF in all scenarios considered.

This article is a starting point for further work in the field of heterogeneous traffic state estimation. For example, this work demonstrates that enhanced particle filtering techniques can improve the accuracy of heterogeneous traffic state estimation, and explored the performance as a function of the traffic regime. A rigorous analysis on model observability and/or error boundedness (e.g., extensions to (Blandin et al. 2012) and (Sun and Work 2018) for heterogeneous traffic models) is challenging but could provide theoretical insights on expected filter performance. Moving towards realistic deployment settings, the functional form of the velocity function will also be important questions to consider. Finally, field data that records more complex heterogeneous traffic scenarios would be insightful to evaluate the performance of the proposed filters when it becomes available.

Acknowledgement

This material is based upon work supported by the National Science Foundation under Grant No. CMMI-1853913 and the USDOT Dwight D. Eisenhower Fellowship program under Grant No. 693JJ31945012.

References

Aw, A., and M. Rascle. 2000. "Resurrection of "Second Order" Models of Traffic Flow." *SIAM Journal on Applied Mathematics* 60 (3): 916–938. https://doi.org/10.1137/S0036139997332099.

Benzoni-Gavage, S., and R. M. Colombo. 2002. "An n-Populations Model for Traffic Flow." *European Journal of Applied Mathematics* 14: 587–612.

Blandin, S., A. Couque, A. Bayen, and D. Work. 2012. "On sequential data assimilation for scalar macroscopic traffic flow models." *Physica D: Nonlinear Phenomena* 241 (17): 1421 – 1440. http://www.sciencedirect.com/science/article/pii/S0167278912001339.

Boel, René, and Lyudmila Mihaylova. 2006. "A compositional stochastic model for real time freeway traffic simulation." *Transportation Research Part B: Methodological* 40 (4): 319–334. https://ideas.repec.org/a/eee/transb/v40y2006i4p319-334.html.

Bowman, Adrian W., and Adelchi Azzalini. 2000. *Applied Smoothing Techniques for Data Analysis: The Kernel Approach with S-Plus Illustrations*. Vol. 15. New York: Oxford University Press Inc.

Chalons, C., M. L. Delle Monache, and P. Goatin. 2017. "A conservative scheme for non-classical solutions to a strongly coupled PDE-ODE problem." *Interfaces and Free Boundaries* 19 (4): 553–570. https://hal.inria.fr/hal-01070262.

Chen, Z. 2003. "Bayesian Filtering: From Kalman Filters to Particle Filters, and Beyond." *Statistics* 182.

Chiarello, F. A., and P. Goatin. 2019. "Non-local multi-class traffic flow models." *Networks and Heterogeneous Media* 14: 371.

Costeseque, G., and A. Duret. 2016. "Mesoscopic multiclass traffic flow modeling on multi-lane sections." In *Proceedings of the 95th annual meeting transportation research board - TRB*, Washington DC, United States, Jan., 27. https://hal.archives-ouvertes.fr/hal-01250438.

Daganzo, Carlos F. 1994. "The cell transmission model: A dynamic representation of highway traffic consistent with the hydrodynamic theory." *Transportation Research Part B:*

Methodological 28 (4): 269 – 287. http://www.sciencedirect.com/science/article/pii/0191261594900027.

Daganzo, Carlos F. 1995. “The cell transmission model, part II: Network traffic.” *Transportation Research Part B: Methodological* 29 (2): 79 – 93. http://www.sciencedirect.com/science/article/pii/019126159400022R.

Doucet, A., and A. Johansen. 2009. “A Tutorial on Particle Filtering and Smoothing: Fifteen Years Later.” *Handbook of Nonlinear Filtering* 12.

Fan, S., and D. B. Work. 2015. “A Heterogeneous Multiclass Traffic Flow Model with Creeping.” *SIAM Journal on Applied Mathematics* 75 (2): 813–835.

Ferrara, A., S. Simona, and S. Silvia. 2018. *Freeway traffic modelling and control*. Springer International Publishing.

Garavello, M., K. Han, and B. Piccoli. 2016. *Models for Vehicular Traffic on Networks*. Vol. 9 of *AIMS Series on Applied Mathematics*. American Institute of Mathematical Sciences.

Gashaw, S., P. Goatin, and J. Härri. 2018. “Modeling and Analysis of Mixed Flow of Cars and Powered Two Wheelers.” *Transportation research. Part C, Emerging technologies* 1–44. https://hal.inria.fr/hal-01708005.

Gazis, D. C., and C. H. Knapp. 1971. “On-Line Estimation of Traffic Densities from Time-Series of Flow and Speed Data.” *Transportation Science* 5 (3): 283–301. https://doi.org/10.1287/trsc.5.3.283.

Godunov, S.K. 1959. “A-difference method for numerical calculation of discontinuous solutions of the equations of hydrodynamics.” *Mat. Sb. (N.S.)* 47(89): 271–306. http://mi.mathnet.ru/msb4873.

Hegyi, A., D. Girimonte, R. Babuska, and B. De Schutter. 2006. “A comparison of filter configurations for freeway traffic state estimation.” In *Proceedings of 2006 IEEE Intelligent Transportation Systems Conference*, Sep, 1029–1034.

Hill, Peter D. 1985. “Kernel estimation of a distribution function.” *Communications in Statistics - Theory and Methods* 14 (3): 605–620. https://doi.org/10.1080/03610928508828937.

Kaipio, J., and E. Somersalo. 2006. *Statistical and computational inverse problems*. Vol. 160. Springer Science & Business Media.

Kanagaraj, Venkatesan, Gowri Asaithambi, Tomer Toledo, and Tzu-Chang Lee. 2015. “Trajectory Data and Flow Characteristics of Mixed Traffic.” *Transportation Research Record* 2491 (1): 1–11. https://doi.org/10.3141/2491-01.

Krajewski, Robert, Julian Bock, Laurent Kloeker, and Lutz Eckstein. 2018. “The highD Dataset: A Drone Dataset of Naturalistic Vehicle Trajectories on German Highways for Validation of Highly Automated Driving Systems.” In *2018 21st International Conference on Intelligent Transportation Systems (ITSC)*, 2118–2125.

Li, L., R. Jiang, Z. He, X. (Michael) Chen, and X. Zhou. 2020. “Trajectory data-based traffic flow studies: A revisit.” *Transportation Research Part C: Emerging Technologies* 114: 225 – 240. http://www.sciencedirect.com/science/article/pii/S0968090X19312987.

Lighthill, M. J., and G. B. Whitham. 1955. “On kinematic waves II. A theory of traffic flow on long crowded roads.” In *Proceedings of the Royal Society of London. Series A. Mathematical and Physical Sciences*, Vol. 229, 317–345. https://royalsocietypublishing.org/doi/abs/10.1098/rspa.1955.0089.

Mallikarjuna, C., and K. R. Rao. 2009. “Cellular automata model for heterogeneous traffic.” *Journal of Advanced Transportation* 43 (3): 321–345. https://onlinelibrary.wiley.com/doi/abs/10.1002/atr.5670430305.

Martino, L., V. Elvira, and F. Louzada. 2017. “Effective sample size for importance sampling based on discrepancy measures.” *Signal Processing* 131: 386 – 401. http://www.sciencedirect.com/science/article/pii/S0165168416302110.

Mihaylova, L., R. K. Boel, and A. Hegyi. 2007. “Freeway traffic estimation within particle filtering framework.” *Automatica* 43: 290–300.

Mihaylova, L., A. Hegyi, A. Gning, and R. K. Boel. 2012. “Parallelized Particle and Gaussian Sum Particle Filters for Large-Scale Freeway Traffic Systems.” *IEEE Transactions on*

Intelligent Transportation Systems 13 (1): 36–48.

Mohan, R., and G.Ramadurai. 2019. "Multi-class Traffic Flow Model Based on Three-Dimensional Flow-Concentration Surface." In *Proceedings of the 98th annual meeting transportation research board - TRB*, Washington DC, United States, Jan., 19–04534. https://trid.trb.org/view/1573120.

Nair, R., H. S. Mahmassani, and E. Miller-Hooks. 2011. "A porous flow approach to modeling heterogeneous traffic in disordered systems." *Procedia - Social and Behavioral Sciences* 17: 611 – 627. http://www.sciencedirect.com/science/article/pii/S1877042811010937.

Ngoduy, D. 2008. "Applicable filtering framework for online multiclass freeway network estimation." *Physica A: Statistical Mechanics and its Applications* 387 (2-3): 599–616.

Ngoduy, D., and R. Liu. 2007. "Multiclass first-order simulation model to explain non-linear traffic phenomena." *Physica A: Statistical Mechanics and its Applications* 385 (2): 667 – 682. http://www.sciencedirect.com/science/article/pii/S0378437107007911.

Ngoduy, D., and A. Sumalee. 2010. "Adaptive Estimation of Noise Covariance Matrices in Unscented Kalman Filter for Multiclass Traffic Flow Model." *Transportation Research Record* 2188 (1): 119–130. https://doi.org/10.3141/2188-13.

NGSIM. 2006. "The Next Generation Simulation Program." http://ops.fhwa.dot.gov/trafficanalysistools/ngsim.htm. U.S. Department of Transportation Federal Highway Administation.

Olivier, L.E., B. Huang, and I.K. Craig. 2012. "Dual particle filters for state and parameter estimation with application to a run-of-mine ore mill." *Journal of Process Control* 22 (4): 710 – 717. http://www.sciencedirect.com/science/article/pii/S0959152412000583.

Polson, N., and V. Sokolov. 2018. "Bayesian Particle Tracking of Traffic Flows." *IEEE Transactions on Intelligent Transportation Systems* 19 (2): 345–356.

Richards, P. I. 1956. "Shock Waves on the Highway." *Operations Research* 4 (1): 42–51. https://doi.org/10.1287/opre.4.1.42.

Risso, M. A., N. Bhouri, A. J. Rubiales, and P. A. Lotito. 2020. "A constrained filtering algorithm for freeway traffic state estimation." *Transportmetrica A: Transport Science* 16 (2): 316–336. https://doi.org/10.1080/23249935.2018.1549618.

Seo, T., A. M. Bayen, T. Kusakabe, and Y. Asakura. 2017. "Traffic state estimation on highway: A comprehensive survey." *Annual Reviews in Control* 43: 128 – 151. http://www.sciencedirect.com/science/article/pii/S1367578817300226.

Simon, D. 2006. *Optimal State Estimation*. John Wiley & Sons, Inc.

Sun, Y., and D. B. Work. 2018. "Error bounds for Kalman filters on traffic networks." *Networks & Heterogeneous Media* 13 (2): 261–295.

Sun, Y., and D.B. Work. 2017. "Scaling the Kalman filter for large-scale traffic estimation." *IEEE Transactions on Control of Network Systems* 5 (3): 968–980.

Surace, S.C., A. Kutschireiter, and J. Pfister. 2019. "How to Avoid the Curse of Dimensionality: Scalability of Particle Filters with and without Importance Weights." *SIAM Review* 61 (1): 79–91. https://doi.org/10.1137/17M1125340.

Szeto, M. W., and D. C. Gazis. 1972. "Application of Kalman Filtering to the Surveillance and Control of Traffic Systems." *Transportation Science* 6 (4): 419–439. https://doi.org/10.1287/trsc.6.4.419.

Tang, T.Q., H.J. Huang, S.G. Zhao, and H.Y. Shang. 2009. "A new dynamic model for heterogeneous traffic flow." *Physics Letters A* 373 (29): 2461 – 2466. http://www.sciencedirect.com/science/article/pii/S0375960109005799.

van Lint, J.W.C., S. P. Hoogendoorn, and A. Hegyi. 2008. "Dual EKF State and Parameter Estimation in Multi-Class First-Order Traffic Flow Models." *IFAC Proceedings Volumes* 41 (2): 14078 – 14083. http://www.sciencedirect.com/science/article/pii/S1474667016412486.

van Lint, J.W.C., S. P. Hoogendoorn, and M. Schreuder. 2008. "Fastlane: New Multiclass First-Order Traffic Flow Model." *Transportation Research Record: Journal of the Transportation Research Board* 2088.

van Wageningen-Kessels, F., H. van Lint, K. Vuik, and S. Hoogendoorn. 2015. "Genealogy of traffic flow models." *EURO Journal on Transportation and Logistics* 4 (4): 445–473. https://doi.org/10.1007/s13676-014-0045-5.

Vivas, C., S. Siri, A. Ferrara, S. Sacone, G. Cavanna, and F. R. Rubio. 2015. "Distributed consensus-based switched observers for freeway traffic density estimation." In *2015 54th IEEE Conference on Decision and Control (CDC)*, 3445–3450. IEEE.

Wang, R., Y. Li, and D. B. Work. 2017. "Comparing traffic state estimators for mixed human and automated traffic flows." *Transportation Research Part C: Emerging Technologies* 78: 95 – 110. http://www.sciencedirect.com/science/article/pii/S0968090X17300517.

Wang, Y., and M. Papageorgiou. 2005. "Real-time freeway traffic state estimation based on extended Kalman filter: a general approach." *Transportation Research Part B: Methodological* 39 (2): 141 – 167. http://www.sciencedirect.com/science/article/pii/S0191261504000438.

Wang, Y., and D. B. Work. 2019. "Heterogeneous traffic estimation with particle filtering." In *2019 IEEE Intelligent Transportation Systems Conference (ITSC)*, 2551–2556.

Work, D. B., O.-P. Tossavainen, S. Blandin, A. M. Bayen, T. Iwuchukwu, and K. Tracton. 2008. "An ensemble Kalman filtering approach to highway traffic estimation using GPS enabled mobile devices." In *Proceedings of 2008 47th IEEE Conference on Decision and Control*, Dec, 5062–5068.

Wright, M., and R. Horowitz. 2016. "Fusing Loop and GPS Probe Measurements to Estimate Freeway Density." *IEEE Transactions on Intelligent Transportation Systems* 17 (12): 3577–3590.

Zhang, H. M. 2002. "A non-equilibrium traffic model devoid of gas-like behavior." *Transportation Research Part B: Methodological* 36 (3): 275–290. https://ideas.repec.org/a/eee/transb/v36y2002i3p275-290.html.

Zhang, PENG, RU-XUN LIU, S. C. WONG, and SHI-QIANG DAI. 2006. "Hyperbolicity and kinematic waves of a class of multi-population partial differential equations." *European Journal of Applied Mathematics* 17 (2): 171–200.

Zhang, Peng, S.C. Wong, and Chi-Wang Shu. 2006. "A weighted essentially non-oscillatory numerical scheme for a multi-class traffic flow model on an inhomogeneous highway." *Journal of Computational Physics* 212 (2): 739 – 756. http://www.sciencedirect.com/science/article/pii/S0021999105003542.

Zhang, Peng, S.C. Wong, and Zhenli Xu. 2008. "A hybrid scheme for solving a multi-class traffic flow model with complex wave breaking." *Computer Methods in Applied Mechanics and Engineering* 197 (45): 3816 – 3827. http://www.sciencedirect.com/science/article/pii/S0045782508001175.